MULTI-MISSION EARTH ENTRY VEHICLE IMPACT ANALYSIS

Nicole C. Bauer[(1)], Brandon P. Smith[(2)], Christopher L. Tanner[(3)], David A. Spencer[(4)]

[(1)]Georgia Institute of Technology, Atlanta, Georgia 30332-0150 USA, Email: nbauer3@gatech.edu
[(2)]Georgia Institute of Technology, Atlanta, Georgia 30332-0150 USA, Email: bpsmith@gatech.edu
[(3)]Georgia Institute of Technology, Atlanta, Georgia 30332-0150 USA, Email: christopher.tanner@gatech.edu
[(4)]Georgia Institute of Technology, Atlanta, Georgia 30332-0150 USA, Email: david.spencer@aerospace.gatech.edu

ABSTRACT

Analyses were performed on the Multi-Mission Earth Entry Vehicle (MMEEV), which uses a foam absorber to safely return a payload to Earth. Using both analytical and computational approaches, these analyses investigate two performance metrics – stroke length and payload acceleration. Performance metrics were analyzed computationally using the finite element solver LS-DYNA. Impact velocity and material properties were varied in order to gauge their influence on the impact performance metrics. Parameter ranges were established using engineering judgment and baseline values from similar analyses completed for Mars Sample Return. From this sensitivity analysis, it was seen that stroke and loading from an impact with an energy absorber are sensitive to impact velocity, forebody density, ground density, and the foam stress-strain curve. Therefore a response surface equation (RSE) was derived through a regression analysis involving these variables. The RSE permits rapid performance analysis of energy absorbing systems using a similar geometry and within material property bounds.

1. INTRODUCTION

The Earth Entry Vehicle (EEV) was proposed as part of the Mars Sample Return (MSR) mission as a simple, reliable capsule that used a passive energy absorber instead of a more complex parachute system to safely return a payload to the Earth's surface [1]. The energy absorber concept consisted of hexagonal foam-filled cells with composite walls assembled in a sphere around a spherical payload. The Multi-Mission Earth Entry Vehicle (MMEEV) [2] uses a similar passive energy absorbing system but is meant to be robust and responsive to various sample return missions, not just from Mars. The MMEEV uses a spherical payload but exchanges the discrete foam cells for one hemi-spherical piece of foam as the energy absorber. A diagram of the MMEEV is shown in Fig. 1.

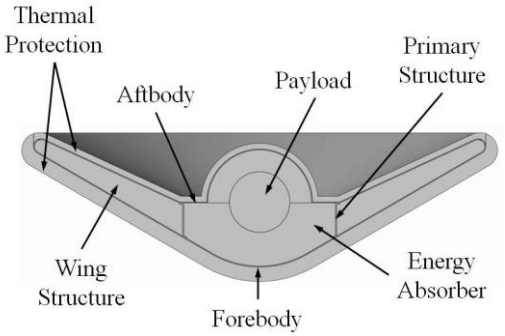

Fig. 1. MMEEV diagram.

The purpose of the energy absorbing system is to limit the maximum acceleration witnessed by the payload to a mission-specific amount. The amount of material crushed upon impact, referred to as stroke length, must be sufficiently thick to prevent complete failure of the absorber material. However, the absorber thickness can be constrained by the vehicle's shape and size, which can have subsequent effects on the payload's acceleration profile. This investigation focuses on the energy absorbing system of the MMEEV and its performance relative to two critical metrics: the payload's peak acceleration and the absorber's stroke length.

To investigate the absorber's performance, a finite element model of the MMEEV was created and analyzed for various loading scenarios and material properties. Loading scenarios include a range of impact velocities into surfaces ranging from soft soil to rigid surfaces. Material properties were varied for the energy absorber foam, the impact surface, and the vehicle's forebody. Finite element results were amalgamated and regressed to construct response surface equations (RSEs) for each performance metric. These RSEs allow for a quick, first-order estimate of the vehicle's final landed state for use in preliminary mission design.

2. FINITE ELEMENT ANALYSIS DESCRIPTION

2.1. Analysis Code

The commercial solver LS-DYNA was used to perform finite element analyses on the MMEEV. LS-DYNA is a non-linear explicit code that exhibits good stability for problems experiencing large deformations and has been extensively used for dynamic impact problems in both the automotive and aerospace fields.

2.2. Model Description

To reduce finite element construction and analysis time, only those components related to the impact absorbing system of the MMEEV were modeled. This model, shown in Fig. 2, includes the payload, primary structure, foam, forebody, and the impact surface. The thermal protection systems and aftbody were assumed to have negligible influence on the performance of the energy absorber.

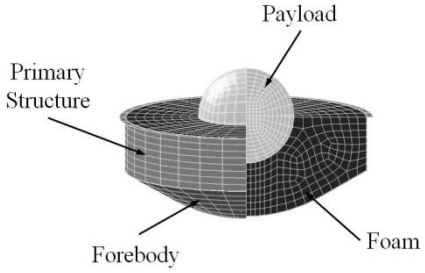

Fig. 2. Finite element model of MMEEV energy absorber system.

The spherical payload is modeled using hexahedron solid elements with a high-modulus, homogeneous linear elastic material (*MAT_001) to create a rigid body. The payload is 13.3 cm in diameter and has a density of 4,000 kg/m^3. The acceleration of the payload was monitored at seven nodes -- six at the extremities of the sphere and one at the center. Nodal displacement was recorded at 4 kHz and differentiated using a 2nd-order central differencing to obtain nodal acceleration.

The primary structure and forebody were modeled using quadrilateral shell elements with two through-thickness integration points. Although the baseline material for the primary structure and forebody is a carbon-carbon composite, sufficient data was not available to develop a representative model. The primary structure was instead modeled using a linear elastic material (*MAT_001) assuming an elastic modulus of 1.03x10^5 MPa [3] and a Poisson's ratio of zero. Although this material model is significantly different that it should be, a simple linear elastic material model was sufficient for the primary structure, which serves as a relatively static structural member. The forebody, however, experiences significant deformation and was modeled using an elastic-plastic material (*MAT_028) assuming the properties of aluminum. To help mitigate uncertain material properties, a wide range of material values was investigated around the assumed values for aluminum to determine the model's sensitivity to the forebody properties.

The energy absorber foam was modeled using over 4,500 hexahedron solid elements. The baseline absorber material is Rohacell® 110WF foam, which is a polymethacrlimide foam with a nominal density of 110 kg/m^3. The most simple, representative material model for the energy absorber was a crushable foam model (*MAT _063), which required unavailable data relating the material's stress to its volumetric strain. Using surrogate foam data [4], an appropriate curve was estimated and parameterized for use in this study. Parameterization of the stress-strain curve is discussed further in Section 3.1.

The baseline ground material is soil at the Utah Training and Test Range (UTTR). The soil was modeled as an isotropic elastic-plastic material (*MAT_012) to best match the available UTTR soil data obtained for MSR EEV analysis [5] and to minimize the complexity of the model while generating realistic deformation behavior. The ground was modeled using over 46,000 hexahedron solid elements to ensure that boundary conditions had a minimal influence on the soil's response. Fig. 3 shows the ground with respect to the MMEEV model.

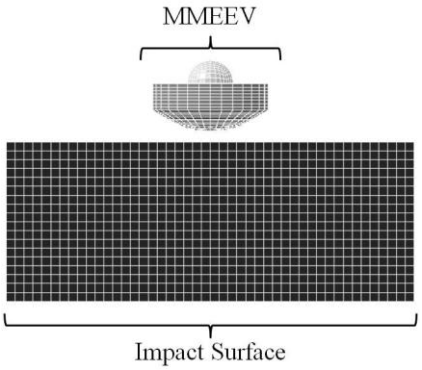

Fig. 3. MMEEV and ground finite element model.

3. SENSITIVITY ANALYSIS

The model performance metrics were tested for sensitivity to variation in material properties and impact velocities in order to choose which design variables to vary in the regression analysis. This simulation investigated the maximum and minimum

Table 1. Minimum, maximum, and baseline values for sensitivity analysis.

Part	Material Property	Maximum	Minimum	Baseline
Forebody	Density (kg/m^3) [6]	19300	1740	2770
	Elastic Modulus (GPa) [6]	300	14	73
	Poisson Ratio [6]	0.42	0.07	0.35
	Yield Stress (MPa) [6]	242	17.8	48.3
	Hardening Modulus (GPa)* [7]	1.00	0.005	0.5
Rohacell Foam	Density (kg/m^3) [8]	300	31	110
	Elastic Modulus (Mpa) [8]	332.0	62	167.5
Soil	Density (kg/m^3) [9,10,5]	2092	881	1486
	Yield Stress (kPa)* [5]	138	0.69	68.9
	Hardening Modulus (kPa)* [5]	1600	8	800
	Bulk Density (kPa) [9,10,5]	2.24E+05	8.69E+04	1.55E+05
	Shear Modulus (kPa) [9,10,5]	2.30E+04	1.38E+03	1.54E+03
	Velocity (m/s) [2]	40.4	30.3	35.5

* Indicates Range Not Found in Literature

values for ground, forebody, and foam material properties. The investigated ranges of material properties and impact velocities are documented in Table 1.

Minimum and maximum values of material properties were established for each part of the model. Soils considered include low density dry sand [9], high density in-situ moisture sand [9], high density flooded sand [9], unwashed sand (clayey sand) [9], soil from Cuddeback Lake, California [10], and wet soil from Carson Sink, Nevada [10]. Metals investigated for the forebody include lead, titanium, beryllium, magnesium, and gold [6]. Foam material property ranges are extracted from published Rohacell® data [8]. If a material property range could not be found in literature, the parameter of interest was varied ±99% from the baseline value in order capture a broad scope of sensitivities. The impact velocity range corresponds to those tested in prior MMEEV analysis [2].

3.1. Foam Constitutive Behavior

The lack of detailed data on the stress-strain behavior of Rohacell® foam presented an additional challenge to this study. The stroke and acceleration behavior of the model depends directly on the input foam stress-strain relationship provided to LS-DYNA. Since this relationship is not well defined in the literature, the foam stress-strain curve was parameterized and varied for the sensitivity analysis. A wide range of stress-strain curves was investigated.

The foam stress-strain relationship was initially modeled after the MMEEV high-density polyurethane foam, but it was found that LS-DYNA was interpreting this input curve in an unexpected manner. The deformation of a single solid element was investigated in order to precisely define how LS-DYNA interprets the input stress-strain relationship. A comparison of the input curve derived from polyurethane and the curve output by LS-DYNA is shown in Fig. 4.

Output strain was calculated with Eq. 1 where γ represents volumetric strain, V symbolizes current volume, and V_i corresponds to initial volume [11]. Current volume (V) was evaluated from element displacement, and element stress was tracked and extracted directly from LS-DYNA output files.

$$\gamma = 1 - V / V_i \tag{1}$$

It is clear that the portion of the foam stress-strain curve corresponding to the sudden jump in Fig. 4 is not resolved in LS-DYNA. Instead, a modified stress-strain curve is generated by the LS-DYNA solver where the strain between the yield stress and compression strength (σ_{max}) is linearly interpolated. Following this behavior, the stress-strain curve in Fig. 5 for a single block element was shown to produce a predictable output. This constitutive model was parameterized and subsequently used for the sensitivity analysis. The initial and final slope are equivalent to the Young's modulus and the yield stress is defined as 86% of compression strength per

the published polyurethane foam data [4]. Finally, a terminal value of stress beyond the compression strength was added to reduce the number of non-physical solutions.

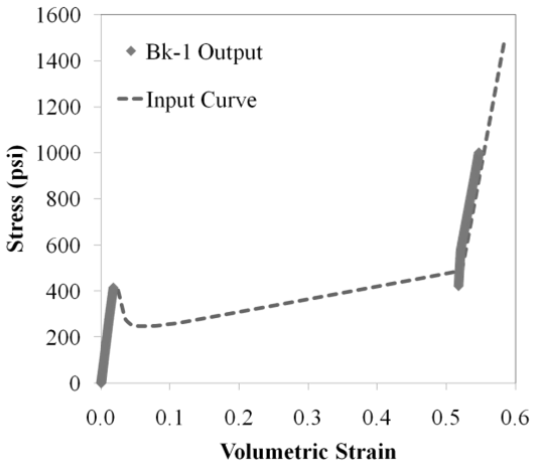

Fig. 4. Comparison of input and output stress-strain models in LS-DYNA for a single finite element block. Bk-1 stands for Block-1.

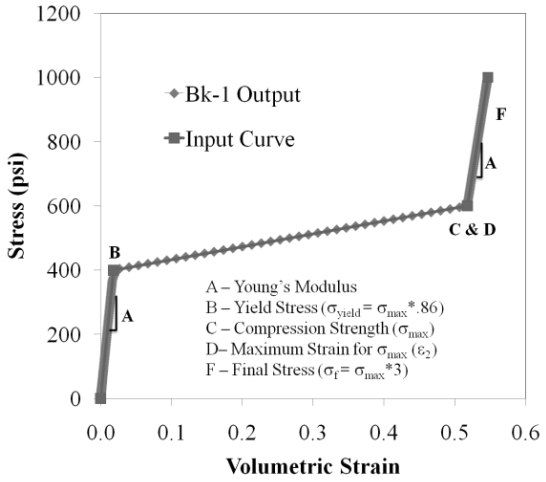

Fig. 5. Parameterized stress-strain curve with predictable behavior. Bk-1 stands for Block-1.

A stress-strain curve was extracted from a single element in the MMEEV model to ensure that the simulation's interpretation of the input stress-strain relationship was as expected. This comparison is shown in Fig. 6. It can be seen here that when the actual stress exceeds σ_{max}, LS-DYNA extrapolates according to the value of Young's modulus (indicated by a dashed line). The loading and unloading data are represented by different symbols. Note that the unloading occurs nearly elastically. This analysis shows that the stress-strain curve can be manipulated by specifying three parameters: Young's modulus, compression strength and strain at σ_{max}.

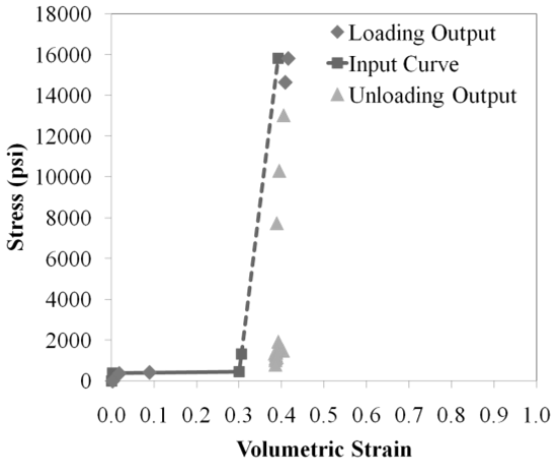

Fig. 6. Input and output stress-strain curve from single finite element block. Dashed line indicates extrapolation.

3.2. Sensitivity Results

The stroke and maximum loading obtained from independent variations of design variables were compared to the performance metrics from the baseline case. If either stroke or maximum loading varied by more than 10%, the model was assumed to be sensitive to that property, and the parameter was included in the regression analysis. The baseline design variables are shown in Table 1 and correspond to an impact into UTTR soil at 40.4 m/s with an aluminum forebody and Rohacell® 110WF foam.

Through this analysis, the model was found to be sensitive to impact velocity, forebody density, soil density, and the foam stress-strain curve (compressive strength, Young's modulus, and strain corresponding to the compressive strength). The selected levels of design variables used for the regression analysis are shown in Table 2.

Table 2. Design variable levels for creation of full-factorial LS-DYNA run matrix.

Design Variable	Levels			
$\rho_{forebody}$ (kg/m^3)	1.94E+4	1.74E+3	1.06E+4	
ρ_{ground} (kg/m^3)	2.09E+3	8.81E+2	1.49E+3	
$\sigma_{max,foam}$ (kPa)	4.40E+2	3.45E+3	7.97E+3	
E_{foam} (kPa)	6.23E+4	1.67E+5	3.32E+5	
$\varepsilon_{2,\ foam}$	0.3	0.5	0.7	
Impact Velocity (m/s)	40.4	30.3	32.8	35.5

4. SURROGATE MODELING

The response surface methodology (RSM) is used to map the stroke and the maximum acceleration response to the design variables. Applying a regression analysis to results from a full-factorial or fractional-factorial run matrix yields simple polynomials that approximate the system response. This surrogate model of the LS-DYNA simulation enables the inclusion of high fidelity impact stroke and acceleration calculations into the end-to-end MMEEV trajectory simulation. Without the RSE, it is difficult to obtain reasonable estimates of the MMEEV structural response in an expedient manner during the preliminary design process.

4.1. Design of experiments

The sensitivity analysis identified six key design variables whose variation caused non-negligible differences in the performance metric responses. A full-factorial run matrix was created from the values listed in Table 2 in order to span the design space and capture interaction between these variables. A total of 972 executions of LS-DYNA were required to generate solutions to the run matrix.

4.2. Simulation Methodology

Each execution of LS-DYNA required approximately 30 minutes using a dual-core 2.4 GHz AMD Opteron processor. With 16 LS-DYNA executions running in parallel, a full-factorial experiment required approximately 31 hours of run time. While this is not a prohibitively long duration, it is evident that the process of input generation, LS-DYNA execution, and post-processing must be fully automated. This was achieved with the three MATLAB functions described below in Fig. 7.

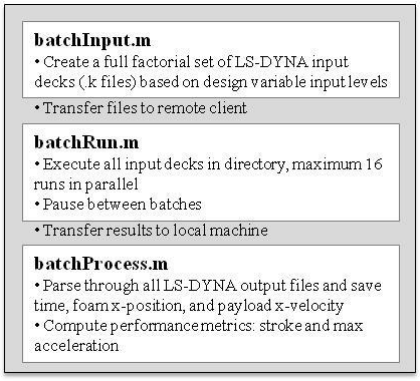

Fig. 7. Description of code to automate LS-DYNA run process with MATLAB.

This framework is made possible with the SSH Toolbox for MATLAB provided by the Ohio Supercomputer Center [12]. This third-party toolbox for MATLAB enables interfacing with the remote client directly from the MATLAB environment. The MATLAB files perform batch operations to create the LS-DYNA input files, execute LS-DYNA, and process the LS-DYNA output. The outputs of this simulation feed directly into the statistical software used for the regression analysis.

4.3. Regression Analysis

The JMP Version 8 statistical analysis software package was used to perform the regression analysis. This software allows the user to rapidly generate RSEs with a variety of methods. The responses generated for this analysis required both logarithmic transformation of the performance metrics and the inclusion of higher order terms. The form of the equations is provided below in Eqs. 2-3 with the design variables defined in Table 3 and regression coefficients shown in Table 4.

$$\begin{aligned}\log10(\text{Stroke}) = \text{Intercept} + \\ (R_{X1}*X1) + \ldots + (R_{X6}*X6) + \\ (R_{XI*X2}*X1*X2) + \ldots + (R_{X5*X6}*X5*X6) + \\ (R_{XI*X1}*X1*X1) + (R_{X6*X6}*X6*X6)\end{aligned} \quad (2)$$

$$\begin{aligned}\log10(\text{Max Acceleration}) = \text{Intercept} + \\ (R_{X1}*X1) + \ldots + (R_{X6}*X6) + \\ (R_{XI*X2}*X1*X2) + \ldots + (R_{X5*X6}*X5*X6) + \\ (R_{XI*X1}*X1*X1) + (R_{X6*X6}*X6*X6)\end{aligned} \quad (3)$$

Table 3. Definitions of design variable shorthand.

Shorthand	Design Variable	Unit
X1	Forebody density	kg/mm^3
X2	Foam max stress	kPa
X3	Foam Young's modulus	kPa
X4	Foam strain at max stress	--
X5	Ground density	kg/mm^3
X6	Impact velocity	mm/s

Table 4. Regression coefficients in RSEs.

Term	Regression Coefficients R_{X1}, R_{X2}, R_{X1*X2}, … Stroke (mm)	Maximum Acceleration (mm/s^2)
Intercept	1.4587634E+00	5.9095825E+00
X1	-2.4907074E+03	-1.7613521E+03
X2	-3.1079607E-04	4.7423093E-08
X3	-3.2987453E-06	2.3021476E-08
X4	5.8393166E-01	-1.2054895E-01
X5	7.2301759E+03	5.0204373E+04
X6	-3.3377131E-07	-4.3137139E-05
X1*X2	-1.8886989E-01	-4.0988362E-01
X1*X3	2.8125311E-03	-3.3037708E-04
X1*X4	-8.2654688E+02	-4.2237817E+02
X1*X5	2.5495816E+09	5.3698277E+08
X1*X6	8.8637803E-02	-6.7766411E-02
X2*X3	-1.5310154E-10	-8.0646870E-12
X2*X4	-6.0472299E-05	1.6784641E-05
X2*X5	1.3966131E+01	4.8891064E+00
X2*X6	-1.0099753E-09	-1.5806193E-11
X3*X4	-4.0479607E-07	9.7718581E-08
X3*X5	4.4135462E-01	-6.1979701E-02
X3*X6	-3.8091096E-11	-3.6247273E-12
X4*X5	3.8534648E+04	-4.1530306E+04
X4*X6	-6.4723221E-06	2.2408111E-07
X5*X6	-2.8039300E+00	-1.2076976E+00
X1*X1	-3.2255349E+07	-6.4778560E+07
X2*X2	2.1964187E-08	-8.1207804E-10
X3*X3	3.8361224E-12	-1.8116346E-13
X4*X4	-3.5881546E-01	6.0760322E-02
X5*X5	-3.5451082E+10	-6.7769640E+09
X6*X6	2.6309158E-11	-4.0322493E-10
Rsquare	**0.980257**	**0.924828**

The RSEs balance a maximum range of validity with minimal error. Two types of model error are investigated in this analysis: model fit error (MFE) and model representation error (MRE). MFE is the error between the data points used to create the RSE and the response. A histogram of the MFE is shown below in Fig. 8 for both responses. The distribution of the mean in both cases appears normal and is centered near 0%. The tails of the stroke error extend beyond 30% in a few cases, while the tails of the max acceleration error extend to approximately 15%. The error in both of these cases is a result of design variable interaction not captured with the 2nd degree linear regression.

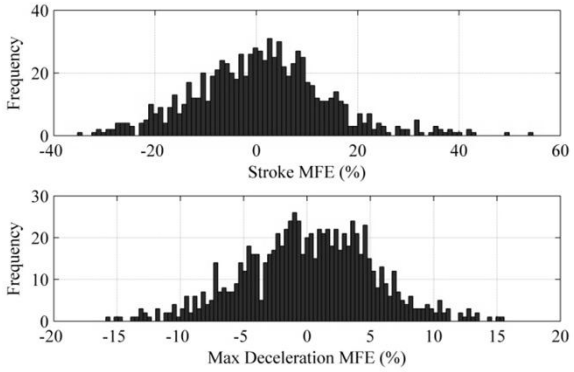

Fig. 8. Model fit error for both responses.

MRE is the error between data points not used to create the RSE. These data provide some indication as to how well the RSE will actually perform when implemented as a subroutine. An additional 96 LS-DYNA cases are generated using design variable levels not included in the RSEs. The error between these cases and the responses are shown below in Fig. 9.

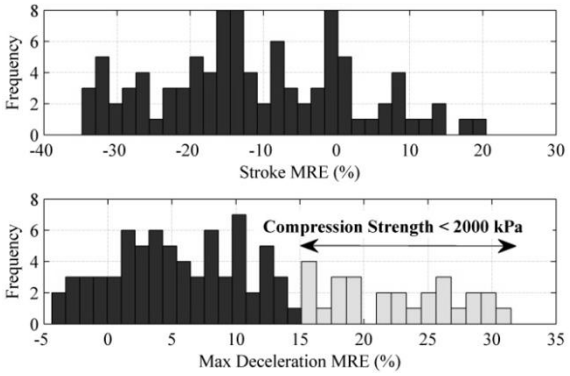

Fig. 9. Model representation error for 96 cases.

The MRE distributions do not appear normal because there are not enough cases represented to resolve the actual statistical model. The stroke MRE lies within the bounds of the MFE, but all cases with compression strength less than 2,000kPa exceed the MFE bounds in the max acceleration response. As discussed in Section 4.6, low compression strengths (440 kPa) often cause the finite element model to break down. For this reason, it is recommended that the RSE provided in this paper be limited to the design variable ranges shown in Table 5 to obtain an estimate for stroke and loading within MRE and MFE.

Table 5. RSE ranges of validity.

Design Variable	Min	Max
X1	1.744E-06	1.938E-05
X2	2000	7970
X3	62280	332730
X4	0.3	0.7
X5	8.806E-07	2.092E-06
X6	-40411	-30302

4.4. Simulation Results

The sensitivities given in Fig. 11 were extracted from the RSE using JMP. In Fig. 11, the scale for stroke and acceleration is log10 to minimize error in the RSE, and the dotted lines correspond to the baseline case. The general trends shown in Fig. 11 follow what was expected out of the sensitivity analysis, and basic physics principles. An explanation for each trend is outlined below:

As the forebody density increases, stroke and maximum acceleration decrease. This occurs because a denser forebody material shields the foam and transfers most of the kinetic energy into soil deformation.

Likewise, a higher foam Young's modulus (steeper slope), causes the soil to deform at a slower rate. This corresponds to a decrease in stroke. Foam Young's modulus does not appear to effect maximum acceleration for the cases considered.

In a similar manner, the foam strain at maximum compression strength, ε_2, is directly related to the amount of deformation. A higher value of ε_2 means that the foam will deform more before the maximum compression strength is reached. As stroke is increased, the foam absorbs the energy that would have otherwise propagated to the payload thereby decreasing the maximum acceleration.

The three parameters that stroke and maximum acceleration are most sensitive to are the density of the ground, the impact velocity, and the compression strength of the foam. The impact velocity and ground density trends follow trends expected from basic physics principles. As the ground density increases it acts like a rigid surface causing an increase in stroke and loading on the vehicle. The same trend is seen with velocity. A high velocity gives the vehicle less time to dissipate kinetic energy from impact, therefore loading and stroke increase.

On the other hand, stroke behaves non-linearly with respect to changes in compression strength, σ_{max}. This behavior stems from the technique LS-DYNA uses to extrapolate the stress-strain values after the absolute maximum stress (σ_f) is exceeded. Essentially the sensitivity trend seen for stroke vs. σ_{max} is a combination of both the Young's modulus and ε_2 sensitivity. This coupling produces a non-linear trend. See Fig. 6 for an example of how the stress-strain curve is extrapolated.

4.5. Limiting Cases

Another objective of the regression analysis was to define the limiting cases for stroke (i.e. where almost all of the foam is crushed and the point where no crush occurs). With a stroke of 66.6 mm and a stroke of 1.67 mm out of 74.6 mm these cases are shown in Fig. 10 and defined in Table 6.

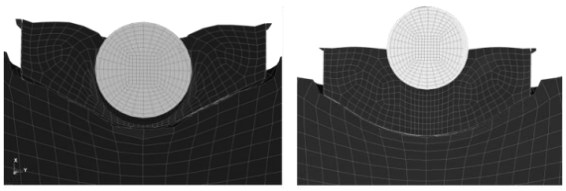

Fig. 10. Extreme values of stroke encountered in simulation.

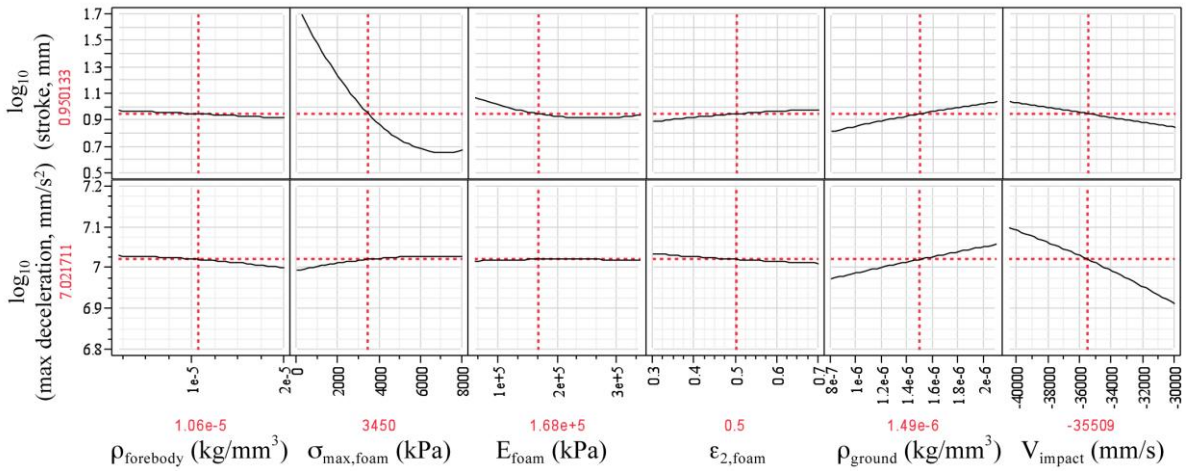

Fig. 11. Model sensitivities to individual RSE inputs

The least stroke corresponds to the stiffest foam and highest forebody density coupled with the lowest ground density and lowest impact velocity. The maximum stroke corresponds to the lowest $\sigma_{max,\ foam}$ and foam Young's modulus, and highest ε_2. Forebody density, ground density, and impact velocity are also at their largest values for the case with maximum stroke.

Table 6. Conditions leading to extreme values of stroke.

Design Variable	Maximum Stroke	Minimum Stroke
$\rho_{forebody}$ (kg/m^3)	1.94E+4	1.94E+4
$\sigma_{max,foam}$ (kPa)	440	7970
E_{foam} (kPa)	6.23E+4	3.33E+5
$\varepsilon_{2,\ foam}$	0.7	0.7
ρ_{ground} (kg/m^3)	2.09E-6	8.81E-7
Impact Velocity (m/s)	-40.4	-30.3
Stroke (% of maximum thickness)	**89.3%**	**2.24%**

4.6. Model Failure

Of the total 972 runs, 15% returned negative volume solutions. Negative volumes were encountered when the impacting layer of foam collapsed on itself rather than compressing the surrounding foam elements. A comparison of the collapsed cells versus a nominal impact is shown in Fig. 12. The only difference between the two impacts is the compression strength (σ_{max}) value. The failure case corresponds to a low σ_{max} of 440 kPa and the nominal case to a σ_{max} of 3,450 kPa. As seen in the figure, the non-physical case bows along the centerline and compresses the bottom layer of elements into itself creating a negative volume which terminates the finite element simulation. For a nominal result, the foam and forebody compress only slightly and deform the surrounding soil. The impact is spread over a larger portion of the impact absorber to dissipate energy more evenly through the vehicle. Conditions for the two cases are given in Table 7.

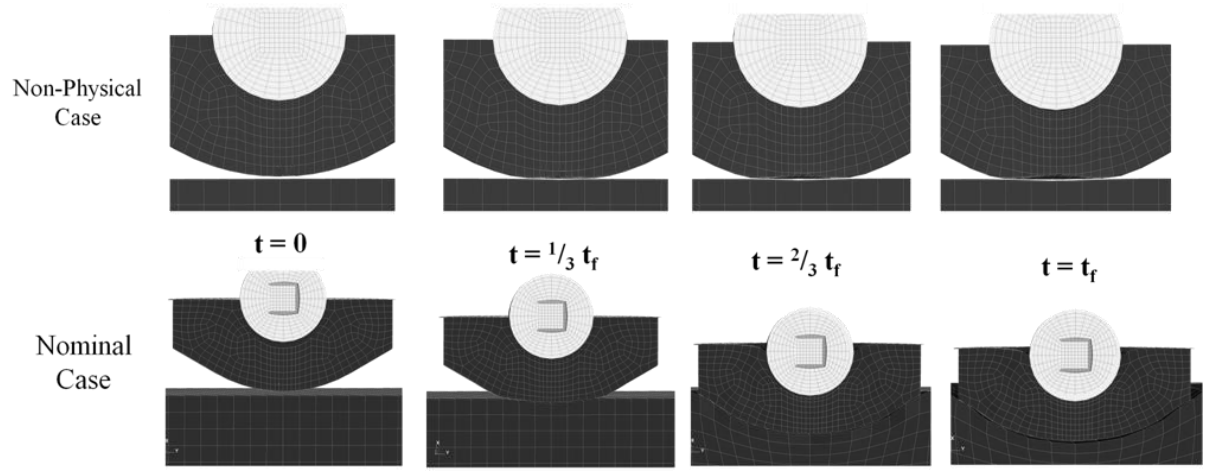

Fig.12 Progression of nominal vs. non-physical impact. The rectangle in center the nominal case payload is only an artifact of image rendering.

Table 7. Conditions for the specified physical and non-physical results.

Design Variable	Nominal	Non-physical
$\sigma_{max,foam}$ (kPa)	3450	440
$\rho_{forebody}$ (kg/m^3)	1.74E+3	
E_{foam} (kPa)	3.33E+5	
$\varepsilon_{2,\ foam}$	0.5	
ρ_{ground} (kg/m^3)	2.09E+3	
Impact Velocity (m/s)	-40.4	

All of the non-physical solutions occurred for either of the two conditions listed below:

- $\sigma_{max,foam}$ = 440 kPa and E_{foam} = 3.32E+05 kPa
- $\sigma_{max,foam}$ = 440 kPa and E_{foam} = 1.67E+05kPa with ε_2 = 0.7

These results indicate that the failure can be traced directly back to the prescribed foam stress-strain curve. A low σ_{max} and high Young's modulus creates a weak foam that may not support itself upon impact. For all Rohacell® foams, a low compression strength corresponds to a low Young's modulus. Therefore the cases themselves are inherently non-physical.

Based on the investigation of the failed cases, and considering the error defined in the regression analysis, σ_{max} should be restricted to a lower bound of 2,000 kPa instead of 440 kPa. This new boundary corresponds to Rohacell® foams 110WF, 200WF, and 300WF as well as many other high density foams. See Table 5 for a full list of bounding conditions.

5. FUTURE WORK

Further analysis will include accommodation for variations in vehicle size and geometry. Further regression analyses will be performed to include these additional design variables in the RSE.

This analysis revealed a few extreme cases where the generated RSE is not valid. Further work is needed to better condition these RSEs and reduce model error. This is particularly necessary for outlying cases, such as those with low compression strength.

6. CONCLUSIONS

A sensitivity analysis completed with the finite element analysis solver LS-DYNA on an MMEEV model showed that stroke and loading from an impact with an energy absorber are sensitive to impact velocity, forebody density, ground density, and the foam stress-strain curve. Bounds were given to each of these properties based on data from the literature, and a full-factorial matrix was created that varied the parameters based on the established boundaries. Using the finite element program LS-DYNA and MATLAB to automate the process, results were generated for a 972 case full-factorial run matrix. These results were then incorporated into a response surface equation using JMP.

The RSE was validated by evaluating its ability to compute stroke and maximum acceleration from 96 cases not included in the original regression. From these spot checks and analysis of the results generated from the 972 cases, the foam compressive strength (σ_{max}) was further restricted to have a lower bound of 2,000 kPa in order reduce error and avoid non-physical solutions.

For a vehicle of similar size and geometry as well as material properties within limits defined in Table 5, the RSE should provide an approximation of the stroke with ±30% error (normal) and maximum acceleration with ±15% error (normal). These estimates can be integrated into a larger design simulation to provide rapid estimates of MMEEV impact performance during the preliminary design process.

7. REFERENCES

1. Mitcheltree, R., Braun, R., Hughes, S., Simonsen, L., "Earth Entry Vehicle for Mars Sample Return," 51st International Astronautics Federation Congress, IAF-00-Q.3.04, Oct 2000.

2. Billings, M. D., "Analytical Simulations of Energy-Absorbing Impact Spheres for a Mars Sample Return Earth Entry Vehicle," AIAA-2001-1602, May 2002.

3. "Carbon-Carbon Thermal Doublers for Spacecraft," Advanced Materials and Processes Technology Newsletter, Vol. 3, No. 2, 1999, pp. 4-5.

4. Kellas, S., "Design, Fabrication, and Testing of a Crushable Energy Absorber for a Passive Earth Entry Vehicle," NASA CR-2002-211425, April 2002.

5. Fasanella, E. L. and Jones, Y. "Earth Impact Studies for Mars Sample Return," *Journal of Spacecraft and Rockets*, Vol. 39, No. 2, March-April 2002, pp. 237-243.

6. MatWeb: Material Property Database. Automation Creations, Inc. <http://www.matweb.com/>.

7. *Strain Hardening*. Web. Feb.-Mar. 2010. <http://aluminum.matter.org.uk>.

8. ROHM GMBH. Qualification Test Data for Rohacell® Grade A and Rohacell® Grade WF to MIL-46194, Part A: Mechanical Properties. 4 July 1997. Raw data. Germany, Qualitatssicherung.

9. Thomas, M.A. et Al., "Constitutive Soil Properties for Unwashed Sand and Kennedy Space Center," NASA CR-2008-215334, July 2008.

10. Thomas, M.A. et Al., "Constitutive Soil Properties for Cuddeback Lake, California and Carson Sink, Nevada," NASA CR 2008-215345, August 2008.

11. LS-DYNA Keyword User's Manual, Version 971, Volume I and II, May 2007.

12. *Ohio Supercomputing Center*. Ohio Board of Regents & State of Ohio. <http://www.osc.edu/>.